Ultrastable and polyamorphic states of vapor-deposited 2-methyltetrahydrofuran Ⓕ

Birte Riechers �ⓘⅅ, A. Guiseppi-Elie, M. D. Ediger ⓘⅅ, and Ranko Richert ⓘⅅ

COLLECTIONS

Ⓕ   This paper was selected as Featured

View Online   **Export Citation**   **CrossMark**

ARTICLES YOU MAY BE INTERESTED IN

Ultrastable and polyamorphic states of vapor-deposited 2-methyltetrahydrofuran

Birte Riechers,[1,a)]   A. Guiseppi-Elie,[2]   M. D. Ediger,[3]   and   Ranko Richert[1]

AFFILIATIONS

[1] School of Molecular Sciences, Arizona State University, Tempe, Arizona 85287-1604, USA

[2] Department of Biomedical Engineering, The Dwight Look College of Engineering, Texas A&M University, College Station, Texas 77843, USA

[3] Department of Chemistry, University of Wisconsin-Madison, Madison, Wisconsin 53705, USA

a) briecher@asu.edu

ABSTRACT

This work reports results gained from dielectric spectroscopy on the organic molecular glass-former 2-methyltetrahydrofuran (MTHF), which was deposited onto an interdigitated electrode device by physical vapor deposition. By a suitable selection of preparation parameters (deposition temperature, deposition rate, and annealing conditions), various states of MTHF could be created: ultrastable glass, a liquid state with unusual dielectric properties, or the ordinary liquid state as obtained by supercooling. Observations on kinetic stability as well as on the suppression of dielectric loss in the ultrastable state resemble previous findings for other molecular glass-formers. Remarkably, after annealing just above T_g, all vapor-deposited films of MTHF display a static dielectric constant in the liquid state (ε_s) that is up to a factor of two below that of the ordinary bulk liquid. A structural transition to the ordinary liquid-cooled state of MTHF occurs at temperatures far above its conventional T_g, indicative of polyamorphism: the formation of an unusual structure that is achieved by physical vapor deposition and that differs from the ordinary liquid state obtained by supercooling. The present results also reveal that the dielectric constant of the as deposited glass (ε_∞) is reduced to practically the value of the squared refractive index, n^2.

Published under license by AIP Publishing. https://doi.org/10.1063/1.5091796

I. INTRODUCTION

Amorphous matter, in contrast to the well-ordered crystalline state, lacks the long-range order even in its solid state. Its preferred motifs are not able to organize in a space-filling fashion, resulting in a frustrated, amorphous arrangement. The conventional way to obtain structurally disordered solids is to cool the liquid material relatively quickly to temperatures below its melting point so that crystallization is inhibited by the lack of time for the molecular rearrangements required for crystal nucleation and growth. A further decrease in temperature of such liquid-cooled samples will eventually result in the transition from the supercooled liquid to the metastable glassy state. The material falls out of equilibrium when structural rearrangements become too slow to restore the thermodynamic equilibrium state, a transition that is marked by the glass transition temperature, T_g.[1] This glass transition is sometimes identified with the system reaching a relaxation time of $\tau = 100$ s or a viscosity of $\eta = 10^{12}$ Pa s. Decreasing the material's temperature below T_g will result in a glassy state with structural and dynamical processes slowly striving toward equilibrium, a process that is denoted as physical aging or structural recovery.[2] In the rare case that more than one glassy or liquid state exists for a single component glass-forming compound, we refer to that situation as polyamorphism. The extension of this term to the liquid state then implies the existence of a liquid-liquid phase transition.

Physical vapor deposition (PVD) facilitates the preparation of amorphous samples following a very different route as the material is deposited from its vapor phase onto a substrate held at a temperature near or below T_g. By controlling the deposition rate and the temperature of the substrate during deposition, the properties of the resulting PVD films can be tuned to display significantly enhanced kinetic stability.[3] Such ultrastable glasses can show extraordinary kinetic and thermodynamic stability,[4–10] higher density,[3,4] restricted degrees of motion such as Johari-Goldstein

(JG) relaxations with reduced amplitudes,[11,12] as well as structural anisotropy.[4,13,14]

The formation of the ultrastable state is based on the enhanced mobility of the surface layers of most recently deposited material due to which molecules are able to sample the topological and energetic landscapes more effectively than is possible for molecules in the bulk material at the same temperature.[15,16] By keeping the deposition rate sufficiently low (typically 1 nm s^{-1} or below), molecules obtain a state that is as close to equilibrium as a liquid-cooled sample might be after ~10^4 or more years of conventional aging, depending on material and annealing temperature.[17] As the deposition continues, molecules become buried and thus immobilized below the surface of the deposited film. Reports on films prepared by physical vapor deposition or comparable techniques cover a range of different materials, e.g., organic molecular glass-formers and metallic glasses. Experiments show that deposition temperatures around 0.85–0.90T_g generally yield glasses with the most pronounced kinetic stability.[18,19] Lower deposition temperatures would limit surface mobility (kinetic control), while higher substrate temperatures would reduce the driving force toward low energy states (thermodynamic control).

Some features of these ultrastable films show behavior that is identical to that expected for liquid-cooled samples aged for a sufficiently long period of time. However, samples prepared by PVD can potentially achieve states that are not accessible via cooling the bulk liquid. For instance, anisotropy has been reported for a number of films produced by PVD.[19–21] Indications of polyamorphism are also found in the literature for vapor-deposited films, e.g., glycerol and other polyols,[22,23] 4-methyl-3-heptanol,[24] and possibly indomethacin.[25,26] Particularly for hydrogen-bonded systems, a change in structure can impact the dielectric properties via the Kirkwood correlation factor, g_K, which can change the dielectric constant at a given dipole density.[27] Therefore, dielectric relaxation experiments are capable of assessing both the dynamics and the structure of liquids and glasses.

The liquid chosen for this study, 2-methyltetrahydrofuran (MTHF), is a glass former of low molecular weight, $M = 86.13$ g mol^{-1},[28] with a caloric glass transition at $T_g = 91$ K.[29,30] The bulk liquid shows little tendency to crystallize at cooling rates as low as 1 K min^{-1}. The temperature dependence of the primary structural relaxation time, $\tau_\alpha(T)$, of supercooled MTHF is characterized by a fragility of $m = \partial \ln \tau_\alpha / \partial (T_g/T)|_{T=T_g} = 65$.[30,31] Due to the molecular dipole moment of 1.58 D,[32] the liquid is polar with a dielectric constant of $\varepsilon_s \approx 17.3$ at about $T = 100$ K.[33–35] The dielectric loss profile is well represented by a Cole-Davidson function, $\varepsilon^*(\omega) = \varepsilon_\infty + \Delta\varepsilon/(1 + i\omega\tau)^\gamma$, with $\gamma \approx 0.5$.[33,36] In the time domain, such dynamics are similar to a Kohlrausch-Williams-Watts decay, $\exp[-(t/\tau)^\beta]$, with stretching exponent $\beta = 0.57$.[37] For MTHF at ambient temperatures (293 K), a density of $\rho = 0.852\,95$ g cm^{-3} and a refractive index of $n_D = 1.4085$ have been reported.[38]

In this work, samples of MTHF were deposited onto an interdigitated electrode device (IDE) by physical vapor deposition and studied by dielectric spectroscopy. At deposition temperatures somewhat below T_g and at moderate deposition rates, kinetically stable glasses were formed. As indicated by the suppression of the residual dielectric loss in this glassy state, packing density was increased relative to the material's state obtained by cooling

the liquid. The as-deposited (AD) glass also displayed a dielectric constant (ε_∞) that was reduced to near the value associated with electronic polarizability ($\approx n^2$). Additionally, the static dielectric constant in the liquid state of vapor deposited films (ε_s) was observed to be about half that of the ordinary bulk liquid, until a structural transition to the ordinary liquid state occurred at temperatures far above the conventional T_g. This latter effect supports the view that physical vapor deposition is an effective tool for studying polyamorphism.

II. EXPERIMENTAL

MTHF (99+%, stabilizer-free, Acros) was used as received, and vapor-deposited films were prepared using a custom-designed setup.[11] The liquid material (max. 5 ml) was kept in a glass reservoir that could be evacuated. The reservoir was connected to the deposition chamber via a shut-off valve, stainless-steel tubing, a regulating needle valve, and another shut-off valve. In preparation for the deposition of MTHF, an antepressure in the order of 0.5–1 mbar was set in the stainless steel tubing to facilitate control of the deposition conditions. The reservoir containing the liquid was shut off during the deposition process as the vapor pressure of MTHF at ambient temperature is too high to ensure sufficiently low deposition rates (<1 nm s^{-1}). The material flow was regulated by using the needle valve that is located at the inlet to the deposition chamber that holds a closed-cycle helium cryostat (Leybold RDK 10-320) to provide the required conditions for vapor deposition onto a cold substrate. The deposition chamber was evacuated to a pressure of ~10^{-6} mbar by means of a turbo pump in addition to the cold finger of the cryostat within the vacuum system. Within the chamber, a radiation shield held at a temperature of 100 K covered the substrate and its holder, with an opening aligned with the inlet for the vapor and facing the substrate. For details, see Fig. S1 in the supplementary material.

An interdigitated electrode device (IDE, Model IME 0550.5-FD-Au, ABTECH Scientific, Inc.), which is a dual-sensing chip with 50 pairs of interdigitated electrodes per sensor on top of a 0.5 mm thick borosilicate glass, served as a substrate.[39] Each digit had a width of 5 μm and a length of 5 mm and was separated by 5 μm from its neighbors. Electrodes consisted of 10 nm Ti/W and additional 100 nm Au sputtered on top. A Si$_3$N$_4$-layer served as protection for the chip's surface, leaving interdigitated electrodes and contact pads exposed. Some experiments were performed with a different IDE (IME 1050.5-FD-Au), for which digit width and spacing were 10 μm. The electrodes on the chips were contacted using a custom-built spring-loaded connector consisting of four Au-pins within a frame made of a Vespel-polymer.

The chip was pressed onto the even surface of a copper block by the springs of the electrical contacts, with a thin layer of Apiezon-N between chip and copper to improve thermal contact. This block was tightly fit into a brass holder that was mounted onto the cold-stage of the cryostat. The temperature was controlled by using a Lakeshore Model 340 using DT-470-CU sensors allowing adjustments in temperature between 30 K and 300 K. Temperature sensors were located on the back of the brass holder and at the cold stage. Temperatures given in the following are based on measurements by using the

sensor located at the brass block that held the sensor chip. To correct for the temperature difference originating from thermal lag (typically in the order of 2 K–5 K), all data of each sample were shifted uniformly so that the loss peak of the experimental data after annealing coincided with the loss peak position of reference data obtained for liquid-cooled (bulk) MTHF measured in a parallel-plate capacitor; see Fig. S2 in the supplementary material.[33]

In order to determine the geometric capacitance, C_{geo}, of each of the two sensors on the chip, 2-ethyl-1-hexanol was used for calibration, where C_{geo} refers to the air/vacuum capacitor that can be filled with the sample material, i.e., excluding the substrate side. Based on its static dielectric constant $\varepsilon_s = 7.61$ at room temperature,[40] the geometric capacitances of the two IDEs were found to be 1.97 pF and 1.94 pF. To be able to determine the permittivity of MTHF when filling the capacitor of the IME 0550.5-FD-Au cell completely, an effective field height H of 2.5 μm was assumed (5.0 μm for the IME 1050.5-FD-Au cell),[41] with the field considered as homogeneous up to $H/2$.[5] If the capacitor were completely filled with the material, the permittivity ε^* on each side (deposition or substrate side) would be determined by the ratio of capacitances using $\varepsilon^* = C^*/C^*_{geo}$. For samples thinner than $H/2$, the relation that connects the incremental capacitance (ΔC) to the observed susceptibility (χ_{obs}) and the film thickness (d) is thus given by

$$\Delta C = C_{geo}\chi'_{obs}(T) = C_{geo}\chi'_{ref}(T) \times \frac{d}{H}, \quad (1)$$

where $\chi_{ref}^*(T) = \varepsilon_{ref}^*(T) - 1$ denotes the reference data.[33] Capacitances were recorded using an Andeen-Hagerling ultraprecision bridge (AH-2700A) connected to one of the two IDEs that are located on the chip, leaving the other one unused.

The temperature protocol of the deposition process and temperature scans is visualized schematically in Fig. 1. After deposition at a specific temperature T_{dep}, the sample was cooled down to $T = 40$ K. For each sample, three successive temperature scans were performed by increasing the temperature in steps of 1.5 K. After the temperature leveled within 0.25 K of the set temperature value for 25 s, dielectric measurements including 8 frequencies between 100 Hz and 20 kHz were conducted prior to approaching the next temperature. After obtaining the final temperature of the first temperature scan at about 100 K, the sample was cooled down to 40 K and kept at that temperature for 10 min. The same procedure was
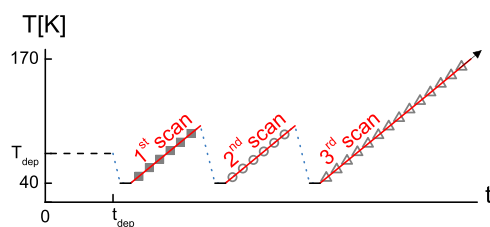
repeated for the second and third scans but with the final temperature of the third scan equal to 295 K to induce desorption of the sample material from the IDE, which typically started at about 140 K.

To correct for the contribution of the borosilicate substrate to the overall capacitance, a temperature scan of the empty chip was conducted with the same thermal protocol as described for the third temperature scan. After subtracting this contribution from data measured at 1 kHz, the resulting values of loss and storage susceptibility, $\chi'_{exp}(T)$ and $\chi''_{exp}(T)$, reflecting the material's response were normalized by dividing by $a = \chi'_{3rd\,scan}(55\,K)/\chi'_{ref}(55\,K)$ for all three temperature scans. As justified further below, this assumes that the annealing during the first and second scans leads to an MTHF glass whose χ' value at $T = 55$ K is virtually identical to the reference obtained by cooling the bulk liquid. By using the relation $d = aH$, the film thickness of the deposited samples was determined and, aided by the duration of the deposition t_{dep}, the deposition rate $r_{dep} = d/t_{dep}$ was deduced.

Films prepared in the manner described above cover the following deposition conditions: deposition temperatures T_{dep} from $0.3T_g$ to $1.2T_g$ using a caloric glass transition of $T_g = 91$ K,[29,30] deposition rates r_{dep} between 0.05 nm s^{-1} and 1.5 nm s^{-1}, and resulting film thicknesses d between 100 nm and 1 μm. The main focus is on films deposited at $0.85T_g$ as well as those with a thickness of 600–700 nm.

III. RESULTS

A. Signatures of stability

The storage (χ') and loss (χ'') susceptibilities for a film prepared at $T_{dep} = 0.84T_g$ are shown in Fig. 2. The susceptibilities of this and all following figures are taken at a frequency of $\nu = 1$ kHz; for the frequency dependence, see Fig. S3 in the supplementary material. The curves reflect typical features of as-deposited PVD films such as the improved kinetic stability that is clearly observed in both the χ'- and the χ''-signal of the first scan relative to the second and third ones. Here, the onset temperature, T_{onset}, as derived from $\chi'(T)$ and indicated in the inset of Fig. 2 is shifted up by 1 K, followed by the transformation from the ultrastable state toward the devitrified state of the material, which is marked by open stars in Fig. 2. The rise in $\chi''(T)$ during the 10 K below T_{onset} could indicate the initial phase of the transformation process. Another well accepted indication for the ultrastable state is observed in the loss contribution of the as-deposited material, where the signal of this glass is clearly suppressed for temperatures below the transformation. These findings indicate an increased packing density in the ultrastable state, analogous to reports for other molecular glass-formers.[11,12] Only when the temperature is elevated beyond the transformation range, the signal of the as-deposited material coincides with that of second and third scans, reflecting a state in which kinetic stability and loss suppression have disappeared by virtue of annealing. Note, however, that the second and third scans are not yet the equivalent of the ordinary supercooled-liquid state as the χ'-plateau has not reached the dielectric constant level of bulk MTHF, $\chi_{SL,ref} = 16.3$. We use the term "ordinary" for the state that would also be achieved by cooling the bulk MTHF liquid from its equilibrium state.

FIG. 1. Schematic representation of the applied temperature protocol throughout deposition and measurement. Dashed line: constant temperature conditions during deposition; dotted lines: cooling procedures with 3.6 K min^{-1}; solid black lines: temperature equilibration of 10 mins duration. Temperature scans (solid red lines with symbols) were conducted with an average heating rate of 0.9 K min^{-1}.

FIG. 2. Experimental results for the storage and loss components of the dielectric susceptibility of MTHF plotted against temperature for three successive temperature scans. Open stars mark the transition range from the ultrastable glass toward the annealed amorphous state during the first scan. The sample was deposited at $0.84T_g$ (indicated by the dotted-dashed line) at a rate of 0.2 nm s^{-1} and has a thickness of 630 nm. The inset shows the definition of the onset temperature for the transition from the ultrastable glass toward the annealed liquid.
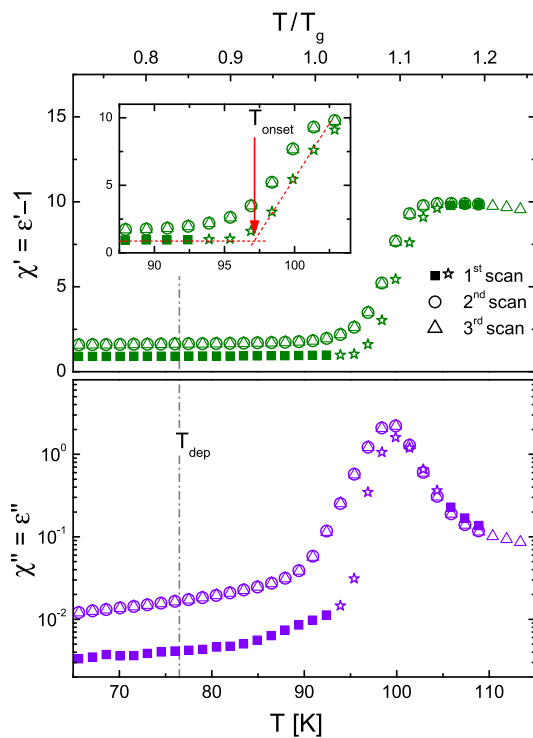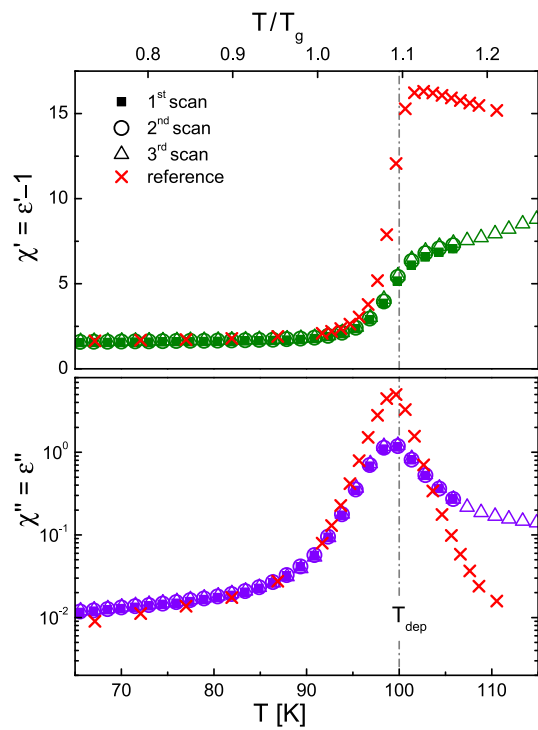

FIG. 3. Experimental results for the storage and loss components of the dielectric susceptibility of MTHF plotted against temperature for three successive temperature scans. The sample was deposited at $1.1T_g$ (indicated by the dotted-dashed line) at a rate of 0.03 nm s^{-1} and has a thickness of 200 nm. Reference data reflecting the ordinary amorphous behavior of liquid-cooled bulk MTHF are included as crosses for comparison.

As demonstrated in Fig. 3, storage and loss data of samples deposited at temperatures above T_g do not exhibit any of the typical features that are connected to the ultrastable state. The signal of the as-deposited sample coincides for both loss and storage contributions with the signal of the second and third scans and thereby shows the same behavior seen in Fig. 2 after annealing. As in the case of Fig. 2, the scans in Fig. 3 do not reflect the ordinary amorphous state, as the comparison to reference data shows. As demonstrated further below, annealing at temperatures in excess of $1.2T_g$ is required in order to recover the ordinary liquid. Therefore, films annealed at temperatures below $1.2T_g$ will be designated as "annealed" to distinguish these from "as deposited" and "ordinary" states.

One method to characterize the degree of kinetic stability of a vapor-deposited glass is the difference, $\Delta T = T_{onset}^{AD} - T_{onset}^{ann}$, between the onset temperatures of the as-deposited (AD) and annealed amorphous ("ann") states. The present study reveals values for ΔT of up to 3.4 K, equivalent to almost 4% of T_g. The resolution of ΔT (see the inset of Fig. 2) is not sufficient to facilitate a quantitative analysis of kinetic stability on the basis of the onset temperatures. Therefore, based on the known correlation between the kinetic stability and suppression of the loss contribution of the as-deposited state,[42,43]

χ''_{AD} may provide a better gauge for the signature of kinetic stability.

To quantify the χ''-suppression that occurs as a consequence of the formation of the ultrastable state, the ratio of the mean values of χ'' between 70 K and 80 K for the first and the subsequent scans, $\chi''_{AD}(70-80\,\text{K})/\chi''_{ann}(70-80\,\text{K})$, was calculated. This ratio, in the following denoted as χ''_{AD}/χ''_{ann}, quantifies the intensity of the χ''-suppression as depicted in Fig. 4, where χ''_{AD}/χ''_{ann} is plotted against reduced deposition temperature (T_{dep}/T_g) and film thickness (d). While a correlation between χ''-ratio and film thickness is not evident, a clear connection of the suppression in χ'' for the as-deposited film with the deposition temperature is observed. This becomes obvious if one focuses on the subset of data that reflects samples with film thicknesses between 600 and 700 nm (orange circles). While films deposited at temperatures as low as $0.3T_g$ do not exhibit any effect on χ'', deposition temperatures around $0.85T_g$ result in minimum values regarding χ''_{AD}/χ''_{ann}. With a further increase in deposition temperature toward T_g, the ratio approaches unity again. Moreover, films deposited at substrate temperatures close to or above T_g result either in the same state as achieved by annealing ($d < 300$ nm) or crystalline films ($d > 700$ nm) so that the ratio χ''_{AD}/χ''_{ann} is close or equal to unity. The observed correlation between χ''_{AD}/χ''_{ann} and the deposition/annealing conditions is in
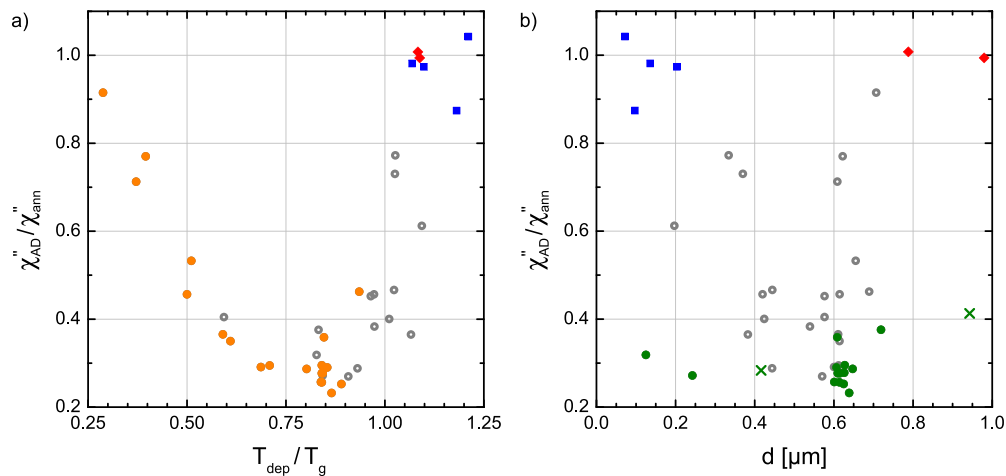
FIG. 4. Experimental results for the loss component ratio, χ''_{AD}/χ''_{ann}, of MTHF plotted against relative deposition temperature (a) and film thickness (b). The data represent samples deposited at rates $r_{dep} < 1.5$ nm s^{-1} in the ultrastable state (gray open circles), the annealed ($T_{dep} > 1.1T_g$) amorphous state (blue filled squares), and the crystalline state (red filled diamonds). Highlighted data points reflect subsets of films with deposition temperatures around $0.85T_g$ (green filled circles) or 600–700 nm thickness (orange filled circles). Green crosses refer to data of upper layers of double-deposition experiments.

very good agreement with experiments on other molecular glass-formers,[19] thus supporting the assumption that vapor-deposited glasses of MTHF have properties similar to other ultrastable glasses.

B. Permittivity in the glassy state

In addition to the known markers of the ultrastable state, another observation is made for vapor-deposited glasses of MTHF that appears to be connected to the PVD technique: Not only the loss but also the storage contribution of the susceptibility, χ', shows a considerable suppression at low temperatures for the as-deposited material. As shown in Fig. 2, the value of χ'_{AD} is as low as 0.88 at temperatures below 80 K, which is significantly below the reference value of $\chi'_{ref} = 1.54$ derived from dielectric measurements on bulk MTHF at $T = 55$ K.[33] This extraordinary effect disappears after annealing the sample toward the liquid state, as can be confirmed by the comparison between first and second or third scans; see Fig. 2. If this annealing process was interrupted prior to completion, i.e., if the final temperature of the first run is set too low to reach the plateau in χ' marking the annealed supercooled liquid state, then also the second run shows a residual suppression of χ' at low temperatures. Thus, only after annealing somewhat above T_g (the condition that would also erase the increased kinetic stability) would subsequent scans coincide with the reference value (bulk MTHF data) in χ' at low temperatures. For samples that were deposited at substrate temperatures too high to create enhanced stability, as in the case of Fig. 3, a suppression of χ' was never observed. Yet, the χ' suppression is not directly linked to kinetic stability or to low χ''_{AD}/χ''_{ann} values because for very low deposition temperatures ($T_{dep} < 0.5T_g$), the suppression in χ' persists, whereas the χ''_{AD}/χ''_{ann} ratios return toward unity as T_{dep} is lowered below $0.7T_g$ [Fig. 4(a)].

Similar to the calculation of the χ''-ratios, the ratio of the mean values of the storage susceptibilities near $T = 55$ K, χ'_{AD}/χ'_{ann}, was determined. The results are plotted against the reduced deposition temperature (T_{dep}/T_g) and the film thickness (d) in Fig. 5, providing an overview of the sample behavior in the investigated parameter regime. Taking into account the projection of the χ'-ratio against film thickness, a correlation becomes obvious, especially when focusing on the subset of samples deposited at $0.85T_g$. Here, for small film thicknesses, the χ'-ratio shows the lowest values which are about $\chi'_{AD}/\chi'_{ann} = 40\%$. The ratio strongly increases with increasing film thickness and levels off for films exceeding 1 μm in thickness (data not shown). The strong correlation between χ'-ratio and film thickness contributes to a rather scattered plot for the projection of χ'-ratio against deposition temperature. Thus, films of 600–700 nm thickness are highlighted in Fig. 5 in the projection of χ'-ratio against deposition temperature. For this subset, rather steady values of the χ'-ratio between 0.5 and 0.6 are observed for deposition temperatures below $0.9T_g$. Unlike the χ'' behavior at low deposition temperatures [see Fig. 4(a) at $T_{dep} < 0.5T_g$], the χ' values remain suppressed even at $T_{dep} = 0.3T_g$; see Fig. 5(a). Elevated deposition temperatures ($T_{dep} > 0.9T_g$) result in an increase in the χ'-ratio and finally in amorphous or crystalline films with less pronounced suppression in χ', i.e., with χ'-ratios closer to unity.

To investigate the connection between the film thickness and the behavior in the χ'-ratio in more detail, a different protocol for deposition and measurement was established. It starts from a film deposited as described before that was measured by two subsequent temperature scans up to about 105 K. Instead of conducting a third scan, the sample was then cooled back to the deposition temperature, and a second layer was deposited onto the already existing film. Deposition parameters were chosen to be comparable for both layers. After the second layer was deposited, another two
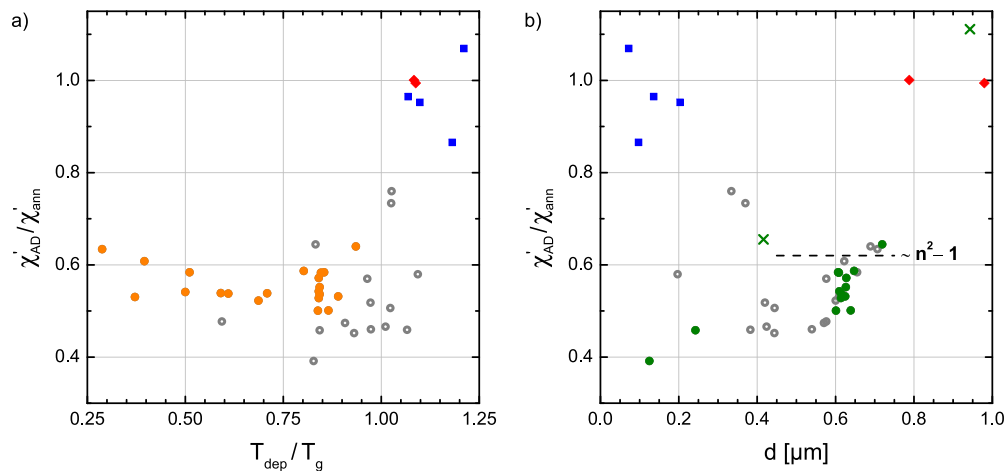
FIG. 5. Experimental results for the storage component ratio, χ'_{AD}/χ'_{ann}, of MTHF plotted against relative deposition temperature (a) and film thickness (b). The data include samples deposited at rates $r_{dep} < 1.5$ nm s^{-1} in the ultrastable state (gray open circles), the annealed ($T_{dep} > 1.1T_g$) amorphous state (blue filled squares), and the crystalline state (red filled diamonds). Highlighted data points reflect subsets of films with deposition temperatures around $0.85T_g$ (green filled circles) or 600–700 nm thickness (orange filled circles). Green crosses refer to data of upper layers of double-deposition experiments. The dashed line indicates the level of $\chi_\infty \approx n^2 - 1$.

temperature scans were measured on the sample. A baseline measurement conducted on the empty IDE served as a correction for the data on the first layer as for previously described measurements. The uncorrected data of the second temperature scan on the first layer served as a correction for the data measured after the second layer was deposited. Normalization of the films occurred as described before, i.e., by dividing the susceptibilities by $a = \chi'_{2nd\ scan}(55\ K)/\chi'_{ref}(55\ K)$ for both temperature scans. Based on this procedure, data on two different double-layer depositions are presented in Figs. 6 and 7.

Storage and loss results for two subsequently deposited layers of MTHF with rather low film thickness of about 200 nm each are compiled in Fig. 6. As the lower part of the graph depicting the loss contribution shows, the first scans of the first and second layers coincide, just as the second scans on the two individual layers do. Features of and differences between the first and second scans are comparable to observations made on single-layer experiments as in Fig. 2. This behavior is in accord with the observation that the χ''-ratio shows no significant correlation with the film thickness as indicated by green crosses for data based on second layers in Fig. 4(b). As the deposition temperature is identical for both layers, significant differences in the χ''-ratios of the individual layers are not expected. The storage contribution presents a similar behavior at first glance: as the upper part of Fig. 6 shows, first and second scans roughly coincide for the two individual layers. However, when taking a closer look at the inset, it becomes clear that even though the suppression of χ'-data is observed in the first scans of both layers, the degree of suppression for the second, upper layer is less intense. If one relates the χ'-ratio to the distance from the substrate rather than to the film thickness itself, the observation of a less intense χ'-suppression during the first scan of the second layer suits the correlation of the χ'-ratio with film thickness, as indicated by green crosses for data based on second layers in Fig. 5.

By comparing a set of layers with higher thickness but comparable deposition parameters as shown in Fig. 7, the correlation of the χ'-ratio to the distance from the substrate becomes even more

FIG. 6. Experimental results for the storage and loss components of the dielectric susceptibility of MTHF plotted against temperature. Two layers were successively deposited at $0.84T_g$ at a rate of 0.30 nm s^{-1} with thicknesses of 242 nm for the first layer (blue symbols and lines) and 173 nm for the second layer (red symbols and lines).
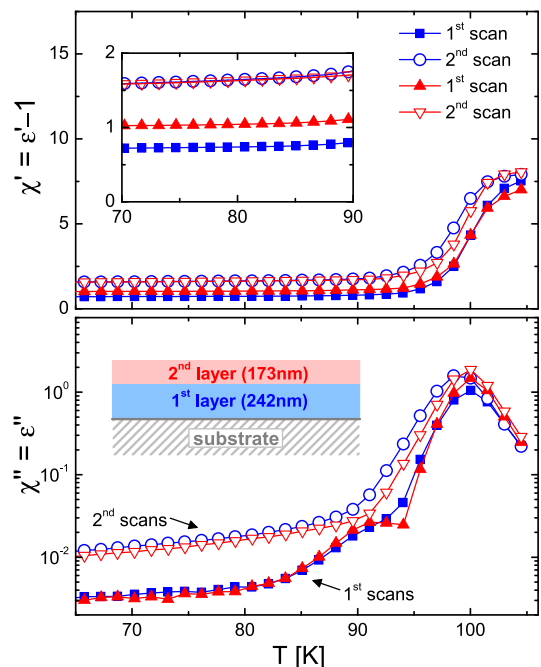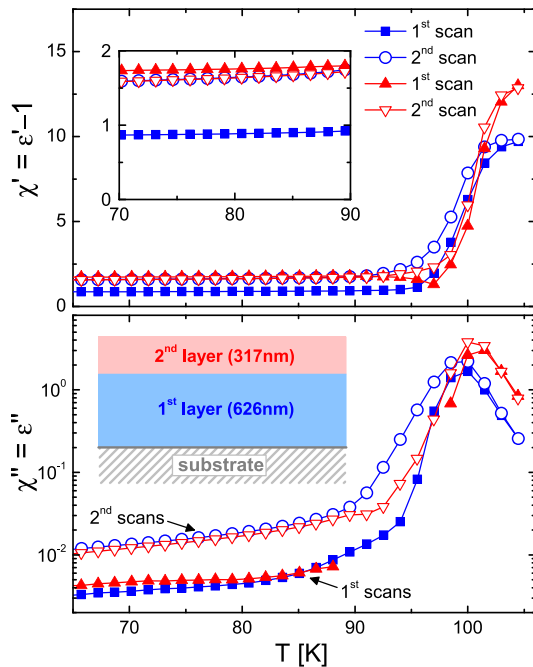
FIG. 7. Experimental results for the storage and loss components of the dielectric susceptibility of MTHF plotted against temperature. Two layers were successively deposited at $0.84T_g$ at rates of 0.25 nm s^{-1} and 0.13 nm s^{-1} and thicknesses of 626 nm and 317 nm for the first layer (blue symbols and lines) and second layer (red symbols and lines), respectively. The gap in the loss data of the second run of the top layer originates from uncertainties involved in subtracting the signal of the underlayer.
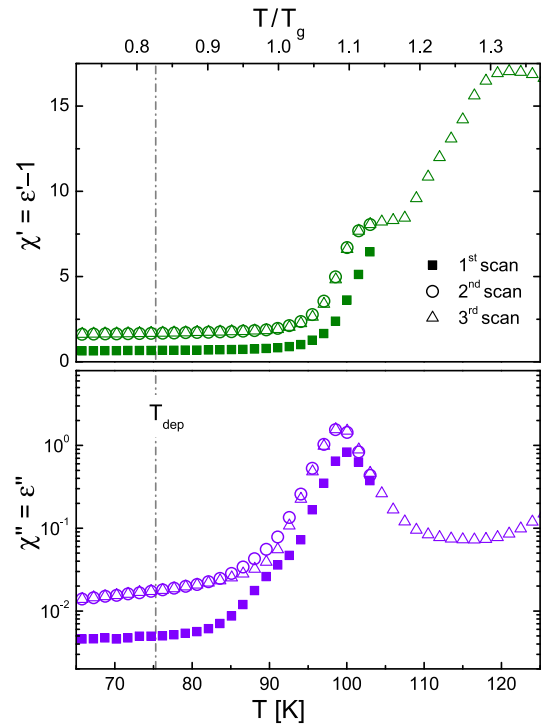

FIG. 8. Experimental results for the storage and loss components of the dielectric susceptibility of MTHF plotted against temperature for three successive temperature scans. The sample was deposited at $0.83T_g$ (indicated by the dotted-dashed line) at a rate of 0.34 nm s^{-1} to a thickness of 125 nm.

obvious. While the loss contribution is comparable for both layers, the storage contributions depict an even more pronounced difference in the χ'-ratio for the individual layers. While the first layer shows a strong suppression in χ' during the first scan, the second layer does not show any suppression in χ', which is in accordance with the observation of a less intense χ'-suppression with larger distance from the substrate's surface (rather than a dependence on film thickness).

C. Permittivity in the liquid state

Another important observation of this work is that the storage contribution of the susceptibility of the annealed liquid, χ'_{ann}, is clearly below the expected value of reference data for the majority of samples. This is depicted in Figs. 2, 3, 6, and 7 which show χ'_{ann} between 7 and 13 for $T > 1.1T_g$, while the reference value is $\chi'_{SL,ref}$ = 16.3 (somewhat below the common maximum of the ordinate scale of 17.5 in all these figures). At first glance, a number of trivial reasons can be thought of to explain this observation: incorrect normalization to reference data, redistribution of the sample material on the sensor chip, or inaccurate baseline subtraction. However, these trivial arguments could be excluded (see the supplementary material for details), and the reproducible measurements on films of about d = 150 nm thickness shown in Fig. 8 strengthen the interpretation of the observed behavior as a physical property of the material.

As shown in Fig. 8, measurements of relatively thin films reveal an additional transition in the storage contribution, yielding a second plateau with an amplitude matching the reference data that represents bulk MTHF. Here, a sample of 125 nm thickness deposited at $0.83T_g$ shows the characteristic behavior discussed before in both the χ'- and χ''-ratios. The second and third scans yield good conformity up to 100 K, suggesting the observation of a well annealed liquid. However, this liquid is not the ordinary liquid, as the low amplitude of the annealed liquid state indicates and as shown by the third scan. The plateaulike development of the data in the third scan around T = 105 K is followed by the storage contribution increasing further, until it reaches a second plateau which matches literature data of the static response of MTHF. This agreement with reference values clearly justifies our cell calibration and the normalization employed to determine the film thickness. The behavior of a clearly established second plateau is only observed in the case of samples that are of comparably low film thickness, i.e., less than 200 nm, while thicker films tend to show a slight increase in amplitude before crystallization sets in. At this point, it shall also be noted that the increase toward the second plateau is not matched by a peak in the loss contribution, thus suggesting that the observed increase in storage amplitude is not due to the onset of a dynamical process but rather due to a transformation of the state of the material.

Further measurements were conducted in order to test whether samples, for which more extensive annealing recovered the permittivity level of the ordinary liquid ($T > 1.3T_g$ in Fig. 8), also showed other properties expected of ordinary supercooled MTHF. To this end, the temperature protocol depicted in Fig. 1 was slightly altered in terms of an increase in the final temperature of the second scan. After deposition of the sample, the initial scan from 40 K to 105 K was conducted resulting in data denoted as "scan A" in Fig. 9. As observed for initial scans in Figs. 2, 3, 6–8, scan A shows a storage contribution of the susceptibility of the annealed liquid, χ'_{ann}, that is clearly below the expected value of the reference data. After cooling to 40 K, the sample was heated toward 121 K during scan B. As in the case of the third scan in Fig. 8, at about 110 K, the signal of the storage contribution starts to increase toward values expected for supercooled liquid MTHF ($\chi'_{SL,ref} = 16.3$). After cooling to 40 K again, the final temperature scan (scan C) was measured up to 167 K. In scan C, the signal in the glassy state is slightly higher than what is expected for the reference data. It is reasonable to assume that the more rapid cooling after scan B captured a glass of higher fictive temperature relative to previous situations: the reference data were obtained at much lower cooling rates, and cooling after scan A began at a significantly lower temperature than after scan B. At temperatures above 105 K, the amplitude of the storage contribution of the annealed liquid, $\chi'_{ann,liq}$, reflects values close to the reference data and agrees well with the signal amplitude achieved with scan B at $T = 121$ K.

Isothermal measurements have been employed to assess the time scales involved in the transitions of χ' from the as-deposited to the annealed level and further to the level of the ordinary state. Samples were deposited under conditions comparable to those of Figs. 8 and 9. Immediately following the deposition process, the samples were heated toward temperature T_{iso}, at which the susceptibility was measured for several 10 000 seconds; see Figs. S6 and S7 in the supplementary material. To observe the transition from the as-deposited to the annealed state, the time scan was conducted at
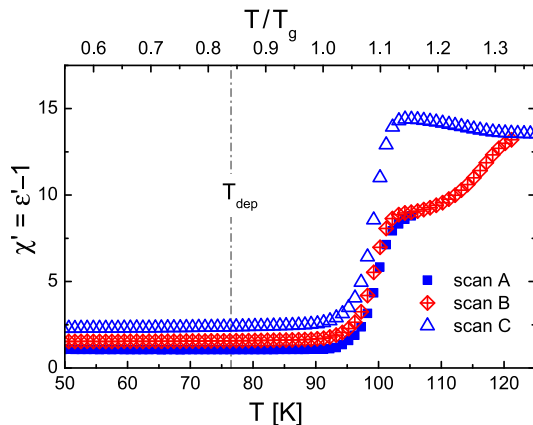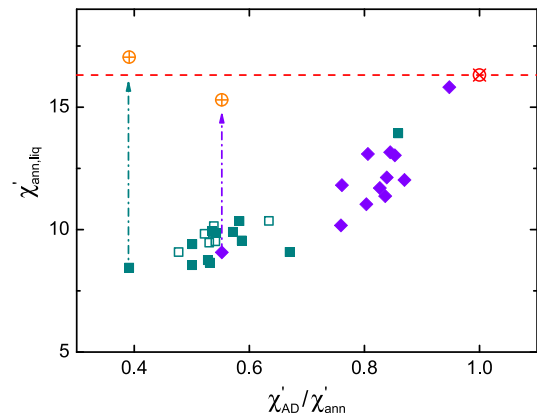

FIG. 10. Experimental results for MTHF depicting the plateau value of the storage dielectric susceptibility of the annealed liquid, $\chi'_{ann,liq}$, vs the ratio χ'_{AD}/χ'_{ann} (55 K) for samples deposited at about $0.85T_g$ (solid symbols, squares and diamonds, are for IME 0550.5 and IME 1050.5 cells, respectively) and for lower deposition temperatures (open symbols). Data are for a variety of film thicknesses and deposition rates. Arrows represent the higher temperature transition to the true ordinary liquid state (orange crossed circles) that displays the dielectric constant of the bulk liquid. The crossed red circle and the dashed line reflect the expected reference value $\chi'_{SL,ref} = \varepsilon_s - 1 = 16.3$.

$T_{iso} = 99.5$ K, a temperature within the range of the observed transition from as-deposited stable glass to annealed liquid (see Figs. 2, 3, and 6–9). The resulting data of χ' vs t reveal an approximately linear increase for about 400 s before it reaches a plateau that reflects the annealed liquid state, $\chi'_{ann,liq}$, i.e., still reduced relative to ordinary MTHF. Another sample was heated to $T_{iso} = 109.5$ K after deposition in order to observe how the annealed liquid recovers the ordinary state in terms of χ'. Here, T_{iso} reflects the onset of the transition process during temperature scans as shown in scan 3 in Fig. 8 and scan B in Fig. 9. Within a duration of approximately 50 s, this χ' vs t curve shows an initial quasilinear increase that covers about one third of the total change of χ'. Then, the signal increases in a more exponential fashion with a half-life of 900 s toward a plateau value that resembles the amplitude of the ordinary liquid state, i.e., the reference level $\chi'_{SL,ref}$.

In Fig. 10, the amplitude of the storage contribution of the annealed liquid, $\chi'_{ann,liq}$, is plotted against the χ'-ratio, χ'_{AD}/χ'_{ann}, for samples deposited at $0.85T_g$ and below. Here, a strong correlation between the χ'-suppression observed for the as-deposited state and the observed amplitude of the plateau during subsequent temperature scans becomes evident. According to the data in Fig. 10, strongly reduced amplitudes of $\chi'_{ann,liq}$ are associated with cases of intense χ'-suppression, while the amplitude of $\chi'_{ann,liq}$ advances toward the reference value of MTHF (dashed line) if the χ'-ratio approaches unity. The variation in the data was triggered either by changes of the deposition rate toward excessive values (~480 nm s^{-1}) or by trace impurities added to the MTHF reservoir.

IV. DISCUSSION

Samples of MTHF were prepared by physical vapor deposition using a broad range of substrate temperatures to investigate

FIG. 9. Experimental results for the storage component of the dielectric susceptibility of MTHF plotted against temperature for three successive temperature scans, using a temperature protocol that deviates slightly from that defined in Fig. 1 (see text for details). The sample was deposited at $0.84T_g$ (indicated by the dotted-dashed line) at a rate of 0.31 nm s^{-1} to a thickness of 176 nm.

the influence of the deposition conditions on the structural state of the material. Relative to the ordinary bulk material, changes regarding (A) the onset temperature and the dielectric loss (or χ'') in the glassy state, (B) the storage susceptibility χ' in the glassy state, as well as (C) the dielectric constant ε_s in the liquid state have been observed in the present PVD study. Only the features listed under (A) are known effects associated with kinetic stability. As the effects in the three different categories respond differently to sample preparation and thermal history, they will be discussed individually below in Subsections IV A–IV C.

A. Signatures of kinetic stability

For numerous materials, the formation of the ultrastable state has been reported to occur after deposition at substrate temperatures between $0.85T_g$ and $0.90T_g$ at deposition rates of 1 nm s^{-1} or less.[19] For these specific deposition parameters, MTHF-samples also show enhanced kinetic stability and a suppression in χ''_{AD} of the as-deposited glass, similar to the ultrastable behavior reported in the literature.[3–12] For many materials, onset temperatures T_{onset} for the transition from the ultrastable to the ordinary amorphous state are in the range of $1.04T_g$–$1.06T_g$.[19,42] As described above, increases in onset temperature ΔT of up to 3.4 K have been observed for vapor-deposited MTHF for deposition temperatures around $0.85T_g$. Accounting for the observation frequency of 1 kHz, these results indicate that MTHF is as kinetically stable as other ultrastable glasses. This is further supported by the long time (400 s) it takes to transform a 100 nm film to the annealed state at $T = 99.5$ K, where the structural relaxation time is about 10^{-4} s.

The ultrastable state is assumed to be close to the state of an ideal glass, where all relaxations have ceased so that the β-relaxation amplitude, $\Delta\varepsilon_\beta$, is expected to go to zero. An experimental example for the suppression of the loss-contribution in the ultrastable glass of toluene reveals a reduction of the β-process amplitude by a factor of 3.4.[11] The temperature range of the most pronounced suppression coincides with that of the most stable behavior as identified by nanocalorimetry heat capacity data,[42,43] suggesting a correlation between χ''-suppression and kinetic stability. In this context, the degree of χ''-suppression for MTHF serves as a quantitative measure for the achievement of the ultrastable state. The reduction of the clearly distinguishable β-relaxation of toluene by a factor of 3.4 indicates a suppression of $\Delta\varepsilon_\beta$ by 70%. As the β-relaxation of toluene is based on molecular reorientations by a cone angle of 2°–10° for 90% of the molecules,[44,45] the observed reduction in β-intensity is discussed to be either due to an elimination of large cone angles or due to a uniform limitation of cone angles by a factor of about 2–3 through an improved packing efficiency in the ultrastable state.[11] Findings for MTHF resemble the degree of suppression reported for toluene, despite the difference in the spectral shape of the loss spectra: a distinct β-process that is well separated from the α-process in the case of toluene but a less pronounced β-wing (excess wing) without a distinct loss peak for MTHF. The similar behavior regarding the β-suppression in the ultrastable states of the different materials suggests that an increased packing density leads to restricted molecular reorientations for MTHF as well, as it is understood to occur for toluene and was reported for a range of other vapor-deposited glass-formers.[11,12,46]

A consequence of the suppression in χ''_{AD} by a factor of 3–4 in the vapor-deposited glass of MTHF, as observed for films deposited at around $0.85T_g$ [Fig. 4(a)], is the decrease in the β-process or excess-wing intensity by about 65%–75%. In accord with Kramers-Kronig-relations,[47] this decrease is reflected in χ'_{AD} by a less intense temperature variation, $\partial\chi'/\partial T$, in the glassy state than what should be observed for samples exhibiting a stronger developed loss-signal. To illustrate this behavior of χ'_{AD} at low temperatures, Fig. 11 shows dielectric data for three different MTHF-samples deposited at $0.3T_g$, $0.85T_g$, and $1.1T_g$. The χ'-contributions of the samples deposited at $0.3T_g$ and $1.1T_g$ show a similar rate of χ' increasing with temperature, consistent with the almost identical loss level for these two cases. By contrast, the ultrastable sample deposited at $0.85T_g$ depicts a clearly diminished temperature-dependence in the storage contribution, along with a concomitant reduction in the level of χ''_{AD}.

Both the shift of the onset temperature and the suppression of the dielectric loss contribution to the secondary or excess wing process observed for MTHF are consistent with known signatures of kinetic stability resulting from vapor deposition. Accordingly, these features are associated with the ultrastable state exhibiting lower enthalpy and higher packing density relative to the ordinary glass.

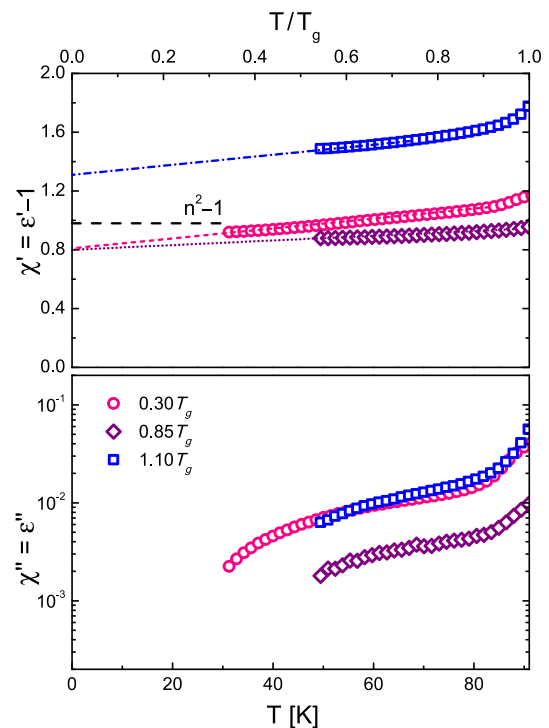**FIG. 11**. Experimental results for MTHF of storage and loss components of dielectric susceptibility reflecting the first temperature scan after deposition plotted against temperature for three different samples deposited at substrate temperatures of $0.30T_g$, $0.85T_g$, and $1.10T_g$. Lines are guides to the eye for storage-contributions at low-temperature. The dashed line indicates the level of $\chi_\infty \approx n^2 - 1$.

B. Reduction of permittivity of the glass

Another important aspect of vapor deposited MTHF is emphasized in Fig. 11, namely, a strong reduction of the glassy value of χ' for samples deposited at $T_{dep} < T_g$. While the samples deposited at $0.3T_g$ and $0.85T_g$ show differences in the intensity of their temperature dependence, both samples extrapolate to a common ordinate value of about $\chi'(T \approx 0$ K$) = 0.80$, a level that is strongly reduced compared to χ' for a sample deposited at $1.1T_g$. This reduction in χ'_{AD} of the glassy state of samples deposited below T_g is reflected similarly in the ratio χ'_{AD}/χ'_{ann}. This reduction occurs independent of the intensity of β-suppression, and it follows a very different temperature- and thickness-dependence than what is observed for the loss-signal due to formation of the ultrastable state (cf. Fig. 5). Therefore, it is regarded as a feature that is not directly connected to kinetic stability. Since Fig. 11 shows that the suppression of β-relaxations is obviously not causing the tremendous drop in χ'_{AD}, the question remains how this strong effect can be understood.

For the films measured in the present setup, density changes due to tighter packing are very small but do not affect the χ'-signal in any case because the deposited samples do not fill the entire capacitor ($d < H$) so that the number of contributing dipoles remains independent of density. Another effect that may influence the amplitude of the dielectric signal is the known tendency of anisotropic molecular orientation for PVD films.[19] In the extreme case of rodlike molecules that arrange their long axis preferentially normal to the substrate surface, a diminishing effect can be estimated that results in a maximum reduction of about 10% of the signal that reflects isotropic packing conditions.[13] Due to the rather isotropic electronic polarizability of MTHF molecules, the effect due to anisotropic molecular packing is expected to be negligible. Thus, an increase in density through enhanced molecular packing efficiency or the occurrence of orientational anisotropy cannot account for the observed reduction in χ'_{AD}, which reaches about 50%.

The reduction of χ'_{AD} observed in the MTHF glassy films is not considered to be spatially uniform. The basis for this notion is that Figs. 6 and 7 [crosses in Fig. 5(b)] show that the χ'-ratio approaches unity with increasing distance from the surface, consistent with the $0.85T_g$ subset of data in Fig. 5(a). Therefore, the dependence on film thickness d should be understood as the result of a gradient of χ'_{AD} normal to the cell surface. Whether the more pronounced χ'_{AD} suppression near the cell surface is a matter of the proximity to the substrate or influenced by the distance dependence of the curvature of electric field lines is unclear at this stage.

In the glassy state, the electronic polarizability is usually a considerable contribution (χ_∞) to the magnitude of χ'. For a molecule with little polarizability anisotropy such as MTHF, this χ_∞ is practically independent of the structure of the material. An approximation to this purely electronic part of χ' is given by the relation $\varepsilon_\infty = \chi_\infty + 1 = n^2$, where n is the refractive index. With $n_D = 1.4085$ for MTHF at room temperature,[38] the structure invariant minimum value is expected to be near $\chi_\infty = 0.98$. According to Fig. 11, the low temperature (high frequency) levels for χ'_{AD} are near or even below this $\chi_\infty = 0.98$ level, which is similarly indicated in Fig. 5(b). This implies that values of χ'_{AD}/χ'_{ann} near 0.5 as observed for MTHF samples of less than 150 nm thickness are equivalent to reducing the residual

relaxational contributions to χ' by a factor significantly exceeding 2 (see Subsection IV C).

The net result regarding χ' is that the values are reduced in as-deposited MTHF glasses, especially in the first few 100 nm s near the substrate, where the ratio χ'_{AD}/χ'_{ann} reaches about 0.5. A clear explanation of this interesting effect cannot be provided until additional results such as ellipsometry become available, but it appears that electronic polarizability dominates the dielectric properties of these films.

C. Evidence of distinct liquid states (polyamorphism)

The values of χ' at $T > T_g$ of the films annealed by scanning up to $1.2T_g$ reach levels of 8 or more, clearly indicating a liquid state that allows for considerable rotational degrees of freedom of permanent dipoles. Although kinetic stability is erased for $T > 1.1T_g$, these $\chi'_{ann,liq}$ values do not reach the permittivity of the ordinary liquid state with $\chi'_{SL,ref} = 16.3$; see Figs. 2 and 3. Instead, these dielectric plateaus observed for temperatures between $1.1T_g$ and $1.2T_g$ remain a factor of around 2 below the reference level $\chi'_{SL,ref}$ of liquid-cooled bulk MTHF.

Because both values of χ', below T_g (cf. Sec. IV.B) and above T_g, are reduced by a factor of about 2, one could speculate that these are correlated features. However, as discussed in Sec. IV.B, the reduction of χ'_{AD} in the glassy state cannot be rationalized by simply scaling the dielectric relaxation amplitude down by a common factor of around 2. It is also worth noting that the suppression of χ' in the glass fades with increasing distance from the substrate, see Fig. 7, whereas the effect above T_g is more distance invariant. Moreover, the unusually low values of χ'_{AD} in the glassy state return to the ordinary level when the temperature reaches about $1.1T_g$ [see Figs. 2 and 5(a)], whereas the reduction to $\chi'_{ann,liq}$ in the liquid state requires annealing at about $1.3T_g$ to be erased (see Figs. 8 and 9). Although the vapor-deposition induced reductions of χ'_{AD} in the glass and $\chi'_{ann,liq}$ of the annealed liquid are not necessarily two signatures of the same unusual state, a connection regarding deposition conditions does exist. As evident from Fig. 10 with focus on films deposited at or below $0.85T_g$, deposition conditions that diminish or eliminate the reduction of χ'_{AD} have the same effects on $\chi'_{ann,liq}$.

Several observations of vapor-deposition induced changes in the relaxation strength, $\Delta\varepsilon = \varepsilon_s - \varepsilon_\infty$, have been reported in the literature: vapor-deposited glycerol and other polyols[22,23] as well as the monohydroxy alcohol 4-methyl-3-heptanol.[24] In these cases, changes in $\Delta\varepsilon$ were connected to a structural reorganization that results in an altered mutual alignment of dipoles. Especially in the case of hydrogen-bonding liquids, changes in supramolecular structures can crucially change the overall dielectric properties of these materials.[48] In contrast to observations made in this work, vapor-deposited 4-methyl-3-heptanol and glycerol exhibit a strong increase in $\Delta\varepsilon$, connected to a more parallel alignment of dipoles in the PVD films relative to the structure found in the ordinary liquid state. The impact of dipole-dipole correlations on the dielectric properties can be quantified by the Kirkwood correlation factor, g_K. It quantifies the change in $\Delta\varepsilon$ by preferred dipole orientations relative to uncorrelated dipoles ($g_K = 1$) at a given dipole density via

$g_K = 1 + z\langle\cos\theta\rangle$, where z is the number of neighboring dipoles and $\langle\cos\theta\rangle$ gauges their average orientation.[47] More parallel dipole alignment ($g_K > 1$) enhances the dielectric constant, whereas antiparallel orientation ($g_K < 1$) has the opposite effect. The Kirkwood correlation factor g_K is related to the dielectric relaxation strength by the Fröhlich-Kirkwood-equation,[47]

$$\frac{(\varepsilon_s - \varepsilon_\infty)(2\varepsilon_s + \varepsilon_\infty)}{\varepsilon_s(\varepsilon_\infty + 2)^2} = \frac{\rho N_A \mu^2}{9 k_B T \varepsilon_0 M} \times g_K, \qquad (2)$$

where N_A is Avogadro's number, k_B is Boltzmann's constant, and ε_0 is the dielectric permittivity of vacuum.

For ordinary liquid-cooled MTHF, the Kirkwood correlation factor was determined to be $g_K = 0.82$ using the values $\varepsilon_\infty = 3.05$,[33] the static dielectric constant based on the reference data $\varepsilon_s = 17.3$,[33] the density $\rho = 0.85$ g cm^{-3},[38] the molecular weight $M = 86.13$ g mol^{-1},[28] the dipole moment $\mu = 1.576$ D,[32] and the temperature $T = 100$ K. This result is fairly close to $g_K = 1$ as it is assumed in the literature,[35] reflecting uncorrelated dipoles for liquid-cooled MTHF. Based on the observed values for the dielectric susceptibility of the annealed liquid state of vapor-deposited MTHF with $\chi'_{\text{ann,liq}} \approx 9$, a Kirkwood correlation factor of $g_K = 0.37$ can be determined. Thus, the diminished $\chi'_{\text{ann,liq}}$-amplitude of the liquid state gained by annealing the vapor-deposited film might be connected to a structure with a preference for antiparallel dipole arrangements, resulting in a cancellation of molecular dipole moments within the capacitor field.

For the annealed films with $\chi'_{\text{ann,liq}} \approx 9$, it should be emphasized that such a deviation of the dielectric constant from the ordinary case at practically constant dipole density is a clear indication of an altered structure, as characterized by the change in g_K. In the case of MTHF, the unusual structure is associated with $g_K < 1$, whereas the mono-alcohol and polyalcohol cases from the previous literature displayed $g_K > 1$.[22–24] Similar to MTHF, vapor deposited amorphous water also displays a lower dielectric amplitude from what is expected from bulk water.[49] There are parallels for the MTHF and glycerol behavior beyond the fact that ε_s is changed for the PVD films annealed just above T_g. In both cases, heating to at least $1.2 T_g$ is required to recover the ordinary liquid state. Also common to both is that an unusual liquid is obtained for all deposition temperatures (including far below T_g).[22]

For the previous vapor-deposited materials that exhibited a deviation in dielectric strength (glycerol, polyols,[22] and 4-methyl-3-heptanol[24]), a recovery of the ordinary behavior of the liquid-cooled material was not observed after annealing just above T_g. Similar to the glycerol case,[22] a transition to the ordinary liquid state occurs at a temperature of around $1.25 T_g$ for relatively thin films of MTHF. As revealed by the data of Fig. 8, the full reference amplitude of liquid-cooled MTHF is reached for $T > 1.3 T_g$, indicative of the structure of the ordinary supercooled liquid. A subsequent scan after reaching a temperature of $1.3 T_g$ demonstrates that this annealing recovers the ordinary behavior of MTHF regarding dielectric constant and dynamics, see scan C in Fig. 9, albeit with a slight increase in χ' in the glassy state due to the faster cooling through T_g. Alternative routes to achieve this state of liquid-cooled behavior for vapor deposited film are given by depositing samples at very high rates ($>10^2$ nm s^{-1}) and, theoretically, by depositing

at temperatures of at least $1.25 T_g$ or by annealing samples showing the reduced χ'-amplitudes at $1.25 T_g$ for sufficiently long times. In practice, however, the last two options are limited by a strong tendency toward crystallization. As samples with a thickness of $d < 200$ nm show the transition toward the supercooled-liquid state of liquid-cooled MTHF in the course of the temperature scans, the time needed for the transformation to complete seems to be sufficiently short so that the amplitude-diminishing effect of crystallization has not yet set in. Such thinner samples also recover the ordinary state level of $\chi'_{\text{SL,ref}}$ upon isothermal annealing at $T_{\text{iso}} = 109.5$ K, and the time scale involved (900 s) is much longer than that of structural relaxation, $\tau_\alpha(T_{\text{iso}}) \approx 10^{-7}$ s. Note that according to the onset temperatures in Fig. 9, both the annealed and ordinary liquids have approximately the same T_g (which is not the result of temperature calibration).

The observed transition from the metastable liquid state gained from annealing the as-deposited films toward the ordinary liquid-cooled behavior suggests that two structurally distinct states of MTHF can be obtained, a situation referred to as polyamorphism.[50] Strictly speaking, however, the dielectric techniques reveal two states with orientational degrees of freedom such that the annealed state could also be a plastic crystal, i.e., a state with a crystal structure regarding the position but with liquidlike rotational dynamics.[51] A further possibility is the heterogeneous mixture of the ordinary liquid with a more nonpolar (possibly solid) phase, analogous to what has been suggested for glycerol.[23] Such a picture would be intrinsically consistent with the similarity of the dynamics of the two states. In any case, structures other than the ordinary state have not yet been reported for MTHF. Both options are associated with the existence of at least two distinct structures with liquidlike orientational mobility, possibly associated with different structures in the respective glassy states. From a theoretical perspective, a first-order phase transition (at $T_{\text{LL}} = 82$ K) that is hidden below the glass transition is expected for MTHF on the basis of the gaussian excitation model advanced by Matyushov and Angell.[52,53] The transition from this unusual amorphous or plastic crystalline state toward the conventional amorphous behavior of the liquid-cooled material at about $1.25 T_g$ marks such a transition from one liquid state to another. Similarly, transitions associated with structural changes occurring well above T_g have been reported for vapor-deposited samples of glycerol and other polyalcohols[22] and of 4-methyl-3-heptanol.[24] While polyamorphism is a phenomenon that has been reported for several bulk materials,[54–60] physical vapor deposition may open new pathways to alternative amorphous states with strongly altered properties for materials that do not show such behavior when prepared by conventional cooling of the liquid.

V. SUMMARY AND CONCLUSION

In this work, we report on the formation of several distinct amorphous states of 2-methyltetrahydrofuran ($T_g = 91$ K) that are gained by vapor deposition onto an interdigitated electrode device at a variety of deposition temperatures T_{dep} and measured by means of dielectric spectroscopy. Deposition at temperatures around $0.85 T_g$ yields the formation of films that are kinetically more stable than the ordinary state of liquid-cooled MTHF. The enhanced kinetic stability is accompanied by a suppression of dielectric loss, ε'', which is

interpreted in terms of an increased packing density that restricts molecular reorientations and thus reduces the amplitude of the β-process or excess wing. Both kinetic stability and suppression of ε'' for MTHF-glasses vapor-deposited around $0.85T_g$ compare well to properties of ultrastable glasses of other materials.

Remarkably, vapor deposition of MTHF results in a reduction of the storage permittivity, ε', of the as-deposited glass. For $T_{dep} < T_g$, this feature is almost independent of T_{dep} and thus not directly connected to the formation of the ultrastable state of MTHF. For samples deposited under these conditions, the high frequency dielectric constant, ε_∞, can be reduced to values as low as the squared refractive index, n^2, corresponding to a significant reduction of residual relaxational contributions at low temperatures. Therefore, the extent of the reduction exceeds what could be explained by effects such as packing density or anisotropic molecular structures. Interestingly, the degree of reduction in ε' is most intense in the proximity of the substrate surface, an effect that is not yet understood. Evidence is provided that these dielectric properties of the glass can be recovered toward those of the ordinary glassy state by annealing via temperature scans that reach $1.1T_g$. For the liquid state reached by this annealing, the amplitude of the storage permittivity ε' clearly indicates orientational mobility but still remains significantly below the value expected for supercooled MTHF. This low ε' occurs after deposition at temperatures from $0.3T_g$ to $1.2T_g$ and remains reduced beyond annealing at temperatures ($1.1T_g$) that would recover ordinary glassy behavior. The amplitude and dynamics of the ordinary liquid are recovered only by annealing thin films ($d \approx 150$ nm) at relatively high temperatures, $T = 1.25T_g$, where the structural relaxation time of MTHF is about 10^{-7} s.

A reasonable explanation for the observed reduction in dielectric amplitude of the liquid is based on assuming a change in dipole-dipole-correlation via g_K, resulting in a net reduction in dielectric amplitude at unchanged dipole density due to a tendency toward antiparallel alignment. We thus conclude that the reduced amplitude of the vapor-deposited liquid state of MTHF is connected to an altered structure that becomes accessible by vapor deposition. It could be interpreted as a form of polyamorphism, created due to the special conditions during vapor deposition. For MTHF, no such unusual state has been reported in the literature.

SUPPLEMENTARY MATERIAL

See supplementary material for additional information on the deposition setup, reference data, frequency-dependence of the glass transition, isothermal annealing, as well as further details on the discussion of the observed amplitude changes.

ACKNOWLEDGMENTS

REFERENCES

[1] M. D. Ediger, C. A. Angell, and S. R. Nagel, J. Phys. Chem. **100**, 13200 (1996).

[2] I. M. Hodge, J. Non-Cryst. Solids **169**, 211 (1994).

[3] S. F. Swallen, K. L. Kearns, M. K. Mapes, Y. S. Kim, R. J. McMahon, M. D. Ediger, L. Yu, and S. Satija, Science **315**, 353 (2007).

[4] A. Laventure, A. Gujral, O. Lebel, C. Pellerin, and M. D. Ediger, J. Phys. Chem. B **121**, 2350 (2017).

[5] A. Sepulveda, M. Tylinski, A. Guiseppi-Elie, R. Richert, and M. D. Ediger, Phys. Rev. Lett. **113**, 045901 (2014).

[6] K. L. Kearns, S. F. Swallen, M. D. Ediger, T. Wu, Y. Sun, and L. Yu, J. Phys. Chem. B **112**, 4934 (2008).

[7] K. R. Whitaker, M. Tylinski, M. Ahrenberg, C. Schick, and M. D. Ediger, J. Chem. Phys. **143**, 084511 (2015).

[8] Y. Z. Chua, M. Ahrenberg, M. Tylinski, M. D. Ediger, and C. Schick, J. Chem. Phys. **142**, 054506 (2015).

[9] H.-B. Yu, Y. Luo, and K. Samwer, Adv. Mater. **25**, 5904 (2013).

[10] J. Q. Wang, Y. Shen, J. H. Perepezko, and M. D. Ediger, Acta Mater. **104**, 25 (2016).

[11] H.-B. Yu, M. Tylinski, A. Guiseppi-Elie, M. D. Ediger, and R. Richert, Phys. Rev. Lett. **115**, 185501 (2015).

[12] C. Rodríguez-Tinoco, K. L. Ngai, M. Rams-Baron, J. Rodríguez-Viejo, and M. Paluch, Phys. Chem. Chem. Phys. **20**, 21925 (2018).

[13] D. Yokoyama, J. Mater. Chem. **21**, 19187 (2011).

[14] S. S. Dalal, D. M. Walters, I. Lyubimov, J. J. de Pablo, and M. D. Ediger, Proc. Natl. Acad. Sci. U. S. A. **112**, 4227 (2015).

[15] J. S. Sharp and J. A. Forrest, Phys. Rev. Lett. **91**, 235701 (2003).

[16] J. D. Stevenson and P. G. Wolynes, J. Chem. Phys. **129**, 234514 (2008).

[17] E. Leon-Gutierrez, A. Sepúlveda, G. Garcia, M. T. Clavaguera-More, and J. Rodríguez-Viejo, Phys. Chem. Chem. Phys. **12**, 14693 (2010).

[18] K. L. Kearns, S. F. Swallen, M. D. Edigar, T. Wu, and L. Yu, J. Chem. Phys. **127**, 154702 (2007).

[19] M. D. Ediger, J. Chem. Phys. **147**, 210901 (2017).

[20] C. Rodriguez-Tinoco, M. Gonzalez-Silveira, J. Rafols-Ribe, A. F. Lopeandia, and J. Rodriguez-Viejo, Phys. Chem. Chem. Phys. **17**, 31195 (2015).

[21] A. Gujral, K. A. O'Hara, M. F. Toney, M. L. Chabinyc, and M. D. Ediger, Chem. Mater. **27**, 3341 (2015).

[22] S. Capponi, S. Napolitano, and M. Wübbenhorst, Nat. Commun. **3**, 1233 (2012).

[23] A. Kasina, T. Putzeys, and M. Wübbenhorst, J. Chem. Phys. **143**, 244504 (2015).

[24] A. R. Young-Gonzales, A. Guiseppi-Elie, M. D. Ediger, and R. Richert, J. Chem. Phys. **147**, 194504 (2017).

[25] K. J. Dawson, K. L. Kearns, L. Yu, W. Steffen, and M. D. Ediger, Proc. Natl. Acad. Sci. U. S. A. **106**, 15165 (2009).

[26] K. L. Kearns, S. F. Swallen, M. D. Ediger, Y. Sun, and L. Yu, J. Phys. Chem. B **113**, 1579 (2009).

[27] W. Dannhauser, J. Chem. Phys. **48**, 1911 (1968).

[28] J.-L. M. Abboud and R. Notario, Pure Appl. Chem. **71**, 645 (1999).

[29] M. Mizukami, H. Fujimori, and M. Oguni, Prog. Theor. Phys. Suppl. **126**, 79 (1997).

[30] R. Richert and C. A. Angell, J. Chem. Phys. **108**, 9016 (1998).

[31] L.-M. Wang, C. A. Angell, and R. Richert, J. Chem. Phys. **125**, 074505 (2006).

[32] M. G. Faizullin, R. V. Galeev, and A. K. Mamleev, Russ. J. Phys. Chem. A **91**, 2275 (2017).

[33] A. I. Nielsen, T. Christensen, B. Jakobsen, K. Niss, N. B. Olsen, R. Richert, and J. C. Dyre, J. Chem. Phys. **130**, 154508 (2009).

[34] R. Richert, Chem. Phys. Lett. **199**, 355 (1992).

[35] C. Streck and R. Richert, Ber. Bunsengesellschaft Phys. Chem. **98**, 619 (1994).

[36] F. Qi, T. El Goresy, R. Böhmer, A. Döß, G. Diezemann, G. Hinze, H. Sillescu, T. Blochowicz, C. Gainaru, E. Rössler, and H. Zimmermann, J. Chem. Phys. **118**, 7431 (2003).

[37] R. Richert, Adv. Chem. Phys. **156**, 101 (2014).

[38] R. Francesconi, A. Bigi, K. Rubini, and F. Comelli, J. Chem. Eng. Data **52**, 2020 (2007).

[39] L. Yang, A. Guiseppi-Wilson, and A. Guiseppi-Elie, Biomed. Microdevices **13**, 279 (2011).

[40] A. G. Gilani, H. Ghanadzadeh, K. Bahrpaima, and A. Ranjkesh, J. Chem. Thermodyn. **42**, 967 (2010).

[41] W. Olthuis, W. Streekstra, and P. Berveld, Sens. Actuators, B **24**, 252 (1995).

[42] K. R. Whitaker, D. J. Scifo, M. D. Ediger, M. Ahrenberg, and C. Schick, J. Phys. Chem. B **117**, 12724 (2013).

[43] M. Ahrenberg, Y. Z. Chua, K. R. Whitaker, H. Huth, M. D. Ediger, and C. Schick, J. Chem. Phys. **138**, 024501 (2013).

[44] M. Vogel and E. Rössler, J. Chem. Phys. **114**, 5802 (2001).

[45] M. Vogel and E. Rössler, J. Chem. Phys. **115**, 10883 (2001).

[46] C. Rodríguez-Tinoco, M. Rams-Baron, K. L. Ngai, K. Jurkiewicz, J. Rodríguez-Viejo, and M. Paluch, Phys. Chem. Chem. Phys. **20**, 3939 (2018).

[47] H. Fröhlich, *Theory of Dielectrics* (Clarendon, Oxford, 1958).

[48] R. Böhmer, C. Gainaru, and R. Richert, Phys. Rep. **545**, 125 (2014).

[49] A. L. Agapov, A. I. Kolesnikov, V. N. Novikov, R. Richert, and A. P. Sokolov, Phys. Rev. E **91**, 022312 (2015).

[50] J. L. Yarger and G. H. Wolf, Science **306**, 820 (2004).

[51] R. Brand, P. Lunkenheimer, and A. Loidl, J. Chem. Phys. **116**, 10386 (2002).

[52] D. V. Matyushov and C. A. Angell, J. Chem. Phys. **126**, 094501 (2007).

[53] D. V. Matyushov, Phys. Rev. E **76**, 011511 (2007).

[54] M. Zhu, J.-Q. Wang, J. H. Perepezko, and L. Yu, J. Chem. Phys. **142**, 244504 (2015).

[55] M. Zhu and L. Yu, J. Chem. Phys. **146**, 244503 (2017).

[56] I. Cohen, A. Ha, X. X. Zhao, M. Lee, T. Fischer, M. J. Strouse, and D. Kivelson, J. Phys. Chem. B **100**, 8518 (1996).

[57] A. Hedoux, Y. Guinet, P. Derollez, O. Hernandez, L. Paccou, and M. Descamps, J. Non-Cryst. Solids **352**, 4994 (2006).

[58] R. Kurita and H. Tanaka, Science **306**, 845 (2004).

[59] H. Tanaka, Phys. Rev. E **68**, 011505 (2003).

[60] H. Tanaka, R. Kurita, and H. Mataki, Phys. Rev. Lett. **92**, 025701 (2004).